RSC Advances

PAPER

Cite this: *RSC Adv.*, 2022, **12**, 19297

Roles of chitosan in synthesis, antibacterial and anti-biofilm properties of bionano silver and gold

Mohammad Aqil M. Fathil, Farha Yasmin Faris Taufeq, Sundos Suleman Ismail Abdalla and Haliza Katas *

Antibiotic-resistance and bacterial bioburden on wound surfaces are the significant challenges to wound healing. Silver and gold nanoparticles (are termed as AgNPs and AuNPs) have been investigated as alternative antimicrobial agents to combat antibiotic-resistant bacterial infections owing to their antibacterial and anti-biofilm activities. Chitosan (CS) has largely been used in nanoparticle synthesis as a stabilizing or capping agent. In this study, AgNPs and AuNPs were synthesized using different concentrations of aqueous extract of tiger milk mushroom (*Lignosus rhinocerotis*) (WETMM) and CS as reducing and stabilizing agent, respectively. Particle size and morphology of both were determined by dynamic light scattering (DLS) method and transmission electron microscopic analysis (TEM). FTIR analysis was conducted to determine the interactions between nanoparticle precursors. The observed peaks at 450 nm and 534–565 nm using a spectrophotometer were corresponded to the surface Plasmon resonance of AgNPs and AuNPs respectively, indicating the formation of respective nanoparticles. FTIR analysis confirmed the role of WETMM as a reducing agent and CS as a stabilizer of AgNPs and AuNPs. Faster formation of nanoparticles was observed besides an increase in particle size when higher CS concentrations were used. TEM micrographs revealed the spherical shape of most nanoparticles with particle sizes in the range of 4 to 58 nm and 18 to 28 nm for AgNPs and AuNPs, respectively. Both nanoparticles exhibited antimicrobial activity against Gram-positive and -negative bacteria, with AgNPs showing a superior antibacterial efficacy than AuNPs. Both microbroth dilution and agar well diffusion assays indicated that CS was an important component to facilitate antibacterial activity for AuNPs. Contrarily, CS stabilization did not enhance the antibacterial efficacy of AgNPs. CS-stabilized AgNPs and AuNPs achieved biofilm inhibition of 53.21% and 79.39% for *Pseudomonas aeruginosa* and 48.71% and 48.16% for *Staphylococcus aureus*, respectively. Similarly, CS stabilization enhanced the anti-biofilm activity of AuNPs but no such effect was seen for AgNPs. In conclusion, CS-stabilized AgNPs and AuNPs possess both antimicrobial and anti-biofilm activities. However, CS acted differently when combined with AgNPs and AuNPs, needing further investigation and optimization to improve the antimicrobial activity of both nanoparticles.

Received 17th March 2022
Accepted 24th June 2022

DOI: 10.1039/d2ra01734b

rsc.li/rsc-advances

Introduction

There is an urgent need to discover efficacious antimicrobial agents as the resistance towards current conventional antibiotics continues to rise. Extensive research on nanotechnology for treating infectious diseases is currently underway as the technology provides a novel way of combating pathogenic resistant bacteria.[1] In the past, silver was used in various ways to kill pathogens.[2] This leads to the discovery of antibacterial properties of heavy metals such as gold and silver. Silver nanoparticles (AgNPs) and gold nanoparticles (AuNPs) have both been developed and tested against Gram-positive and -negative bacteria. With high total surface area to volume ratio and crystallographic surface structure, AgNPs and AuNPs exhibit an excellent antimicrobial activity.[3]

Biofilms are communities of microorganisms, adhered to the surface and protected by a layer of shield comprising of proteins and polysaccharides. Biofilm-producing organisms demonstrated a higher resistance to conventional antibiotics, leading to treatment failure and further development into chronic conditions[4] such as chronic diabetic wounds. Previously, AgNPs demonstrated significant dose-dependent anti-biofilm effect against *Pseudomonas aeruginosa* and *Staphylococcus aureus*.[5] Dual antimicrobial and anti-biofilm effects of AgNPs further reinforce their potential in the fight against resistant pathogenic microbes.

Traditionally, nanoparticles (NPs) are synthesized *via* top-down or bottom-up approach. In the top-down method, bulk

Centre for Drug Delivery Technology, Faculty of Pharmacy, Universiti Kebangsaan Malaysia, Jalan Raja Muda Abdul Aziz, Kuala Lumpur, 50300, Malaysia. E-mail: haliza.katas@ukm.edu.my; Fax: +60-3-26983271; Tel: +60-3-92897971

materials are grinded mechanically until they form nano-sized particles. However, the drawback to this method is that it requires heavy machineries and usually run processes in larger batches, which are not suitable for lab-scale nanoparticle production. On the other hand, the bottom-up approach, or better known as the chemical method, is preferred over the former production style as it usually involves simple chemical reaction and has high conversion rate into small sized NPs.[6] However, chemical reagents that are used to reduce the NPs are mostly harmful to the environment and human health, causing some researchers to steer away from adopting this method in their works. Of late, biological synthesis is the favourable route because it is generally more economical and easily accessible.[3] Various microorganisms and plant extracts were used to synthesize NPs and had proven to be viable options as alternative reducing agents.[7]

Tiger milk mushroom (TMM), or scientifically known as *Lignosus rhinocerotis*, is an edible mushroom with therapeutic qualities and had recently been used to synthesize NPs as a reducing agent.[8] It is found in various parts of the world and is regularly consumed by the indigenous people of Malaysia for its numerous health benefits.[9] Aqueous extract of TMM (WETMM) not only has reducing capacities, it also exhibits antimicrobial activities against various bacterial strains through *in vitro* testing which could potentially enhance the overall antimicrobial effect of AgNPs and AuNPs synthesized.[10] Chitosan (CS) is a biopolymer composed of D-glucosamine and *N*-acetyl-D-glucosamine backbone that are linked together by glycosidic β^{1-4} linkage.[11] CS is a natural polycationic carbohydrate biopolymer and it is used in the synthesis of metal NPs. CS possesses good biodegradability and antibacterial properties which makes it a good stabilizing agent to protect AgNPs and AuNPs from agglomeration and improve biocompatibility of metal NPs.[12]

Despite the use of WETMM and CS for synthesizing AuNPs has been reported previously, there are currently no data that directly compares the antibacterial and anti-biofilm activities of these AuNPs with its less expensive counterpart, AgNPs. The influence of CS on the antimicrobial activity of both NPs is also worth to investigate, as CS itself is known to exhibit antimicrobial activity besides its role in stabilizing the nanoparticles produced. Therefore, this study explored the roles of CS to stabilize and protect the formed NPs from agglomeration and growth in a single pot. AgNPs and AuNPs were biosynthesized using WETMM as a reducing agent and the physicochemical characteristics of both with or without CS stabilization were characterized and compared. Their antibacterial and anti-biofilm activities were also evaluated against common pathogenic bacteria that infect chronic wounds and produce biofilms, namely *Staphylococcus aureus* and *Pseudomonas aeruginosa*, using the microbroth dilution method and the crystal violet assay. The findings of this study would provide a deeper understanding on the role of CS in the production of NPs, with respect to their particle size, zeta potential, and morphology as well as antibacterial and anti-biofilm activities against selected Gram-positive and -negative bacteria.

Materials and methods

Materials

TMM powder (*Lignosus rhinocerotis*) was given as a gift from Lignas Bio Synergy Plt., Selangor, Malaysia. Silver nitrate ($AgNO_3$) (ACS reagent grade) and chloroauronic acid ($HAuCl_4$; gold(III) chloride hydrate) were procured from Sigma Aldrich, Ireland. Low molecular weight CS (LMW: 50–190 kDa, 75–85% deacetylated) was purchased from Sigma Aldrich (Ireland). Ciprofloxacin HCl was purchased from TargetMol, USA. Two bacterial strains (*Staphylococcus aureus* ATCC 25923 and *Pseudomonas aeruginosa* ATCC 27853) were obtained from Microbiology Laboratory of Faculty Pharmacy, Universiti Kebangsaan Malaysia (UKM). All bacterial strains were maintained in broth prior to testing. Mueller-Hinton broth (MHB) and Mueller-Hinton agar (MHA) were purchased from TargetMol, USA. Crystal violet was obtained from Chemiz, UK. 70% ethanol was procured from J-Kollin Chemicals, UK and glacial acetic acid (99.7% purity) was purchased from R&M Chemicals, UK.

Water extraction of TMM (WETMM)

The extraction was carried out according to a previous method.[13] Briefly, TMM powder (25 g) was extracted using 250 mL distilled water at a ratio of 1 : 10 (w/v). The solution was then stirred continuously for 30 min at 60 °C under a magnetic stirring. The solid residues were removed from the solution using a Whatman 150 mm filter paper prior to centrifuging the solution at 10 000 rpm (4 °C) for 15 min (Allegra 64R from Beckman Coulter, Ireland). The supernatant recovered from centrifugation was filtered using a Whatman 150 mm filter paper. The obtained extract solution was freeze-dried using a freeze dryer (ScanVac CoolSafe) at −110 °C to produce lyophilized form of extract. Various concentrations of WETMM solutions (0.05, 0.1, 0.2, 0.8 mg mL^{-1}) were prepared by dissolving in distilled water and kept at 4 °C prior to its use as a reducing agent for the synthesis of AgNPs and AuNPs.

Preparation of biosynthesized AgNPs and AuNPs

CS solutions at different concentrations (0.03, 0.06 and 0.09% w/v) were made in 1% v/v glacial acetic acid. The solutions were sonicated for 15 min at 40 Hz and filtered to obtain clear solutions. Different formulations of AgNPs and AuNPs were prepared by varying WETMM and CS concentrations. Capped AgNPs (Formulations F1–F5) were synthesized according to a method reported previously with some modifications.[12,13] Briefly, 5 mL WETMM (0.05, 0.1, 0.2 and 0.8 mg mL^{-1}) was mixed with 1 mL of 0.01 *M* silver nitrate solution (0.017% w/v) and 5 mL of CS solution (0.03, 0.06, 0.09% w/v). On the other hand, uncapped AgNPs (Formulation F6) were produced by only mixing the silver nitrate solution and WETMM. The reaction was performed at room temperature on standing until the yellow color turned into reddish brown (the target color), indicating the formation of AgNPs. The mixture was sonicated for 20 min, followed by stirring at 300 rpm for 30 min. The resulting mixture was washed three times with deionized water by

centrifugation (15 000 rpm for 15 min) to remove excess unreacted reactants.

The same method was applied to prepare AuNPs except for 1 mL of 0.01 M chloroauronic acid ($HAuCl_4$; gold(III) chloride hydrate) solution was used. The mixture was left at room temperature until the solution turned into purplish color to indicate AuNPs formation. Then, AuNPs solution was sonicated for 2 h at 40 Hz, followed by washing and harvesting by centrifugation at 15 000 rpm for 15 min. The yield of nanoparticles was expressed by the following formula, of which the weight of lyophilised nanoparticles is referred as the actual yield and the total weight of dry materials used are referred as the theoretical yield:

$$\text{Percentage yield} = \frac{\text{actual yield}}{\text{theoretical yield}} \times 100\%$$

The formation of AgNPs and AuNPs was also analyzed using a UV-vis spectrophotometer (Shimadzu 180, Centurion Scientific, New Delhi). The scan range was set at 200–700 nm at a scan speed of 480 nm min^{-1}.

Particle size, polydispersity index (PDI) and zeta potential

The mean particle size (Z-average), PDI, and zeta potential (surface charge) of prepared biosynthesized AgNPs and AuNPs (without dilution) were determined using a Malvern Zetasizer Nano ZS (Malvern Instruments, UK). All measurements for particle size were performed at 25 °C with a detection of angle of 90°. Samples were measured in triplicate and the data were presented as mean ± standard deviation (SD).

XPS measurement

Electronic and chemical structure of AgNPs as well as AuNPs stabilized by CS were analyzed using X-ray photoelectron spectroscopy (XPS) (Kratos AXIS Ultra, UK). X-ray source used in this analysis was Al Kα (1486.6 eV). The deconvolution and curve fitting were done using CasaXPS software. Background signals in the spectra were corrected using the Shirley algorithm before curve fitting. Peak assignments were referenced to the C1s set at 284.6 eV.

Morphology analysis

Morphological analysis of biosynthesized AgNPs and AuNPs was conducted using a transmission electron microscopy (TEM) (Philips, CM12, USA). Prior to analysis, the fabricated NPs were frozen in Lexicon II ULT Freezer at −81 °C for 3 days and lyophilized using a freeze dryer (ScanVac CoolSafe). Then, dried NPs were suspended in distilled water. For the analysis, drops of sample dispersion were placed on the grid and allowed to dry at room temperature for 1 min. The sample was then viewed under TEM at different magnifications.

FTIR analysis

Samples for Fourier transform infrared spectroscopy-attenuated total reflectance (FTIR-ATR) were prepared by suspending lyophilized NPs, WETMM and CS in distilled water. Then, a few drops of samples were placed on the ATR crystal. FTIR-ATR analysis of AuNPs, AgNPs, WETMM, and CS was conducted in the range of 4000–400 cm^{-1} by using a FTIR spectrophotometer (PerkinElmer 100 Spectrum, Walthman, MA, USA). The spectra were acquired using 32 scans and a 4 cm^{-1} resolution.

Antibacterial assays

Inoculum preparation by growth method. *S. aureus* (ATCC 25923) and *P. aeruginosa* (ATCC 27853) were cultured on plates containing MHA using the agar streak method, and then incubated (Memmert, Schwabach, Germany) overnight at 37 °C. Inoculums were prepared by using a sterile loop to aseptically transfer 3–5 colonies of the same morphological type into a universal bottle containing 5 mL MHB. The bacterial suspension was incubated overnight to allow bacterial growth. After 24 h, the turbidity was adjusted spectrophotometrically (UV-vis Shimadzu 180 spectrophotometer) to an absorbance of 0.08–0.13 at 625 nm by adding sterile broth as to obtain a standardized microbial suspension of 1×10^8 CFU mL^{-1} for all bacterial strains.

Agar well diffusion test. Agar diffusion method was used to measure the antimicrobial inhibition zone of *S. aureus* and *P. aeruginosa*. The test protocols were mainly derived from a method previously reported with some adjustments.[14] A concentration of 1×10^8 CFU mL^{-1} for both bacterial strain cultures were prepared and spread on the dried surface of a MHA plate by using a sterile cotton swab. The diluted bacterial solution was swabbed uniformly on the agar surface by repeating twice and rotating approximately 60° each time. The well was made on the plate by using a sterile 6 mm diameter pipette tip. Ciprofloxacin HCl (20 μg mL^{-1} solution and 5 μg disc) and distilled water were used as the positive and negative control, respectively. For sample testing, approximately 40 μL of the different formulations of AgNPs and AuNPs were loaded into different wells by using a micropipette. The plates were incubated at 37 °C for 24 h. The diameter of inhibition zone was measured using a plastic ruler. The measurements were made in triplicate.

Microbroth dilution method. This method was used to determine the value of minimum inhibitory concentration (MIC).[14,15] Serial dilutions were performed from a starting concentration of 1–2 mg mL^{-1} of uncapped AgNPs and AuNPs as well as CS-stabilized AgNPs and AuNPs by using MHB as a diluent. Each dilution reduced the concentration by two folds. Then, a bacterial suspension of 1×10^8 CFU mL^{-1} was prepared by adjusting the overnight bacterial cultures to match the turbidity of standard 0.5 McFarland solution using the UV-vis spectrophotometer. The bacterial suspension was further diluted with MHB at 1 : 100 ratio to obtain roughly 1×10^6 CFU mL^{-1}. Subsequently, 100 μL of each type of bacterial strains was dispensed into each well of 96-well plate containing 100 μL of treatment samples to give a final bacterial concentration of 5×10^5 CFU mL^{-1}. The plates were then incubated at 37 °C overnight. On the following day, the plates were stained using 20 μL

triphenyl tetrazolium chloride (TTC) reagent (0.2% w/v) and the results were obtained by observing the presence of red formazan color. The lowest concentration at which no visible growth (no formation of red color) occurred was noted as the MIC value of the samples.

Anti-biofilm potential. Crystal violet assay was used to determine the efficacy of samples in inhibiting biofilm formation.[16,17] Initially, a standardized bacterial culture with the concentration of $OD_{560} = 0.02$ (1×10^6 CFU mL^{-1}) was prepared. Aliquot (100 μL) of each culture was transferred into the wells of flat-bottomed 96-well plate and incubated for 24 h without shaking for biofilm formation. Then, 100 μL of treatment solutions in six different concentrations (1, 0.5, 0.25, 0.125, 0.0625 and 0.032 mg mL^{-1}) were added into the wells and further incubated at 37 °C for 24 h. Sterile distilled water served as a negative control. After the second incubation, the 96-well plates were washed five times with sterile distilled water and air-dried in the oven at 40 °C for 45 min. A volume of 100 μL of 1% crystal violet solution was added into the wells and incubated at room temperature for 15 min. Then, the plates were washed again three times with sterile distilled water to remove unabsorbed purple stain of crystal violet. After the third wash, biofilms were observed as thin layer of purple gel-like films attached to the side and bottom of the wells. Subsequently, 150 μL of ethanol was added to destain the wells. Finally, 100 μL aliquot of the destaining solution from each well was transferred to a new plate. The absorbance of all the samples were recorded at 590 nm using a microplate reader (Thermo Scientific Multiskan GO). The mean absorbance for each sample was determined, and the percentage biofilm inhibition was calculated using the equation below:[17]

$$\frac{\text{Control } OD_{590}\text{ nm} - \text{treatment } OD_{590}\text{ nm}}{\text{control } OD_{590}\text{ nm}} \times 100\%$$

Statistical analysis

The data acquired are presented as the mean ± standard deviation (SD). The data were analyzed by ONE-way ANOVA followed by Tukey's *post hoc* test. Analyses were computed using GraphPad Prism 6. Values of $p < 0.05$ was considered to indicate a statistically significant difference between the samples tested.

Results and discussion

Formation and characterization of AgNPs and AuNPs

Formation of NPs. AgNPs were formed within 3–5 days, depending on the CS concentrations used. This is one of the known drawbacks of using mushrooms for biosynthesis of AgNPs, that they are generally slow.[3] Previously, by using waste mushroom of *Pleurotus ostreatus* (oyster mushroom) as reducing agents, it took 3 days to convert Ag^+ into Ag.[12] The color of reaction mixture changed from colorless to reddish-brown, indicating the formation of AgNPs (Fig. 1A). The color change took place gradually from light yellow to yellow, and finally reddish brown after 3–5 days depending on the concentration of CS used. The color change was a result of the excitation of surface Plasmon vibrations in the NPs whereby yellow-brown color indicated the formation of AgNPs.[18] The presence of biomolecules such as saccharides and amino acids allows metal ions to bind to their active functional groups, facilitating the reduction of metal ions into 0 oxidation state.[19] AgNPs stabilized by CS (Fig. 1A) appeared to have darker color of solution as compared to AgNPs without CS (uncapped) (Fig. 1B). On top of having stabilizing properties for NPs, CS can also serve as a reducing agent. Since the biosynthesis method involves adding CS at the early stage of reduction, it could have acted together with WETMM and further enhance the reducing capacities. The reducing power of reducing agents increases over time because more OH^- groups are converted to carbonyl groups by air oxidation which in turn reduces the Ag^+.[20] As a result, more AgNPs were formed, and the color of solution leaned more towards brown.

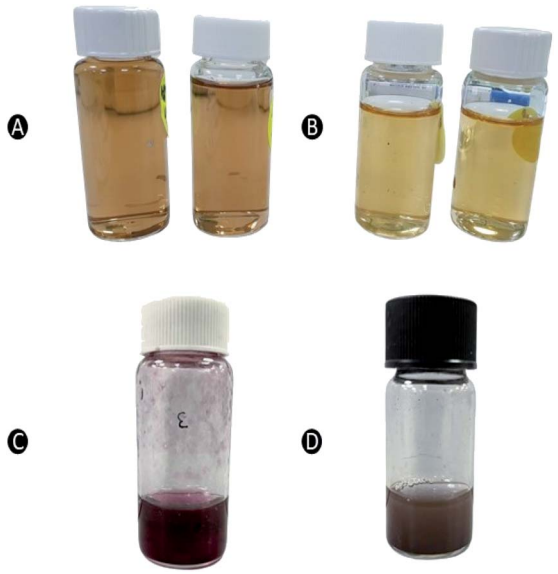

Fig. 1 Color changes in the reaction mixture of (A) capped AgNPs stabilized by CS, (B) uncapped AgNPs, (C) capped AuNPs stabilized by CS, and (D) uncapped AuNPs.

In case of AuNPs, the nucleation occurs within few hours of sonication whereby the initial yellow color turns into dark purplish wine (Fig. 1C and D). Similar to the AgNPs, purple color of AuNPs was more pronounced in formulation that had been added with CS (Fig. 1C) as a stabilizer as compared to the formulation without CS (uncapped) (Fig. 1D). AuNPs changed to the target color (3 h) at a much faster rate as opposed to AgNPs (3 days).

Percentage yield (%) are presented in Table 1. Determination of yield is crucial in minimizing the risk of obtaining low yields with high product expenses. To address these limitations, the study of NPs produced *via* green synthesis has emerged and often relates to a high yield production, which has also been reported to be cost effective, eco-friendly and relatively less toxic, making it a better alternative to chemical synthesis.[3] According to Table 1, the incorporation of CS into the

Table 1 Yield of uncapped AgNPs, uncapped AuNPs, capped AgNPs and capped AuNPs, $n = 3$

Sample	Actual yield (mg)	Theoretical yield (mg)	Percentage yield (%)
AgNP-CS	5.72 ± 0.43	11.2	51.1 ± 3.8
AgNPs	1.27 ± 0.26	4.4	27.0 ± 6.0
AuNP-CS	10.8 ± 0.62	16.8	64.2 ± 3.72
AuNPs	1.1 ± 0.20	5.4	20.3 ± 3.70

fabrication of NPs significantly improved the yield. Furthermore, other than stabilising the NPs, CS as a capping agent was shown to enhance the yield by twofold.

UV-visible spectroscopy analysis. UV-vis spectrophotometry is considered a primary analysis to determine the formation of NPs.[3] The formation of AgNPs was confirmed by the characteristic Plasmon resonance band at 450 nm (Fig. 2A and B).[3] Similar findings can be observed using extract of *Pleurotus ostreatus* waste as reducing agents.[21] The absorption at the wavelength above 400 nm was a typical wavelength for formation of AgNPs due to the intense surface Plasmon resonance.[12,22] The small peak at 270–300 nm area could possibly be due to clusters of Ag^+ and Ag particles during initial stage of reduction.[23] As for the AuNPs counterpart, the formation of AuNPs was confirmed by the presence of the surface Plasmon resonance band at a distinct wavelength peak of 565 nm (Fig. 2C) and 534 nm (Fig. 2D) for uncapped and capped AuNPs, respectively. Generally, the surface Plasmon resonance band for AuNPs formation in the range of 500–570 nm.[3] Similar findings can be seen in previous reports whereby UV spectra of CS-stabilized AuNPs were formed around 530 nm.[24,25] The shift to 534 nm was due to a local change in the refractive index caused by CS coating.[26]

Particle size, PDI and zeta potential

The particle size of different formulations of AgNPs and AuNPs is presented in Table 2. The size of capped AgNPs were significantly smaller than uncapped AgNPs ($p < 0.05$). In previous research involving waste mushroom of *Pleurotus ostreatus* as reducing agents, the NPs were formed first prior to stabilizing with CS, which resulted in significantly larger sizes of AgNPs compared to those formulations without CS.[12] In contrast to this study, the formation and capping of AgNPs all occur at the same time because both CS and WETMM were mixed in silver salt solution. NPs are considered as metastable because when the bulk materials are reduced to nanoscale features, they exhibit much higher energies. In this state, the probability of primary nanostructures to collide and form clusters are very high and if the addition of a stabilizing agent into the AgNPs was delayed, agglomeration would already occur to a certain extent.[27] In this one-pot production method, the immediate presence of CS form self-assembled monolayer[8] to provide stability and thus, resulting in particles with smaller sizes as compared to uncapped AgNPs. Hence, the primary nanostructures of NPs were better preserved due to the optimum use of capping agent, resulting in lower particle sizes for CS-stabilized AgNPs. In

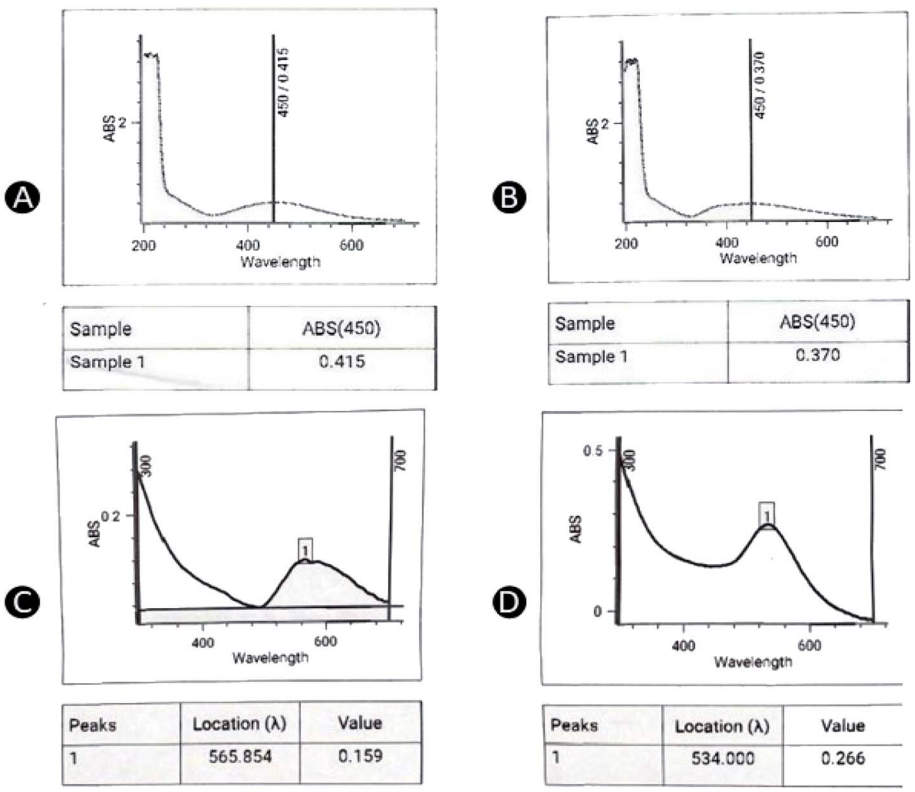

Fig. 2 UV-vis spectrophotometry of (A) uncapped AgNPs, (B) capped AgNPs, (C) uncapped AuNPs, and (D) capped AuNPs.

Table 2 Different formulations of AgNPs and AuNPs and the effect of CS capping or stabilization on the mean particle size, PDI and zeta potential, $n = 3$

AgNPs/AuNPs	Metal ion (M)	WETMM concentration (mg mL^{-1})	CS concentration% (w/v)	Particle size (nm) ± SD		PDI		Zeta potential ± SD	
				AgNPs	AuNPs	AgNPs	AuNPs	AgNPs	AuNPs
F1	0.01	0.2	0.03	125.0 ± 23.7	81.5 ± 3.2	0.50 ± 0.14	0.46 ± 0.21	+25.1 ± 0.37	+35.7 ± 4.42
F2	0.01	0.2	0.06	164.1 ± 36.7	133.5 ± 26.1	0.44 ± 0.02	0.56 ± 0.04	+32.3 ± 2.27	40.5 ± 0.81
F3	0.01	0.2	0.09	191.1 ± 24.0	185.2 ± 13.35	0.42 ± 0.04	0.52 ± 0.04	+37.3 ± 1.83	+35.0 ± 8.46
F4	0.01	0.1	0.09	58.4 ± 6.3	155.2 ± 18.4	0.52 ± 0.03	0.49 ± 0.04	+31.7 ± 4.80	+35.7 ± 4.30
F5	0.01	0.05	0.09	110.4 ± 15.2	173.1 ± 66.8	0.42 ± 0.05	0.40 ± 0.06	+36.6 ± 3.50	+35.7 ± 4.51
F6 (uncapped AgNPs)	0.01	0.1	—	200.9 ± 44.2	—	0.22 ± 0.06	—	−12.2 ± 0.93	—
F7 (uncapped AuNPs)	0.01	0.8	—	—	86.4 ± 14.8	—	0.40 ± 0.05	—	−8.1 ± 1.18

contrast to AgNPs, F1–F5 of AuNPs were mostly larger than uncapped AuNPs (except for F1) which could be due to the lower WETMM concentration (8-fold) used compared to the uncapped one. It should be noted that a higher WETMM concentration was needed to produce NPs for uncapped AuNPs. Similar findings were reported elsewhere in which the particle size of metal NPs increased when CS was added into the formulation.[12] The electrostatic interaction between AuNPs and CS using the one-pot production method probably differs from that of AgNPs whereby CS did not form monolayer, thus hindering its ability to stabilize and repel other NPs from forming agglomerates.

An obvious trend of increasing particle size could be seen with the increase in CS concentration (Table 2). Electrostatic repulsion and interchain hydrogen bonding interactions exist in equilibrium below a certain limit of CS concentration. However, when CS concentration increases, the NH^{3+} surface shielding dominates over the hydrogen bonding during the crosslinking process, causing many CS molecules to link with single particles. As a result, larger particles are formed because electrostatic repulsion between particles is not enough to sustain stability of these large particles.[28] In this case, incorporating the lowest concentration of CS (0.03% w/v) in the formula is ideal as the smallest particle size could be obtained as opposed to formulations F2 and F3. However, CS concentration 0.09% w/v was selected for further testing owing to faster formation of NPs by using this concentration. The formation of AgNPs and AuNPs using 0.09% w/v CS was achieved after 3 days and 3 h, respectively while 5 days and 4 h for 0.03% w/v CS.

Decrease in WETMM concentration from 0.2 (F3) to 0.1 mg mL^{-1} (F4) reduced the particle size of both NPs. However, further decrease in WETMM to 0.05 mg mL^{-1} did not reduce the particle size. Previously, particle size of AuNPs were reported to reduce by decreasing WETMM concentration (0.05 to 0.0125 g mL^{-1}).[8] Hence, F4 (0.01 M Ag, 0.09% w/v CS and 0.1 mg mL^{-1} WETMM) was selected for further analysis. Without CS, the uncapped AgNPs were larger in particle size (200.9 ± 44.2 nm) while the formation of AuNPs could not be detected, suggesting that the formation of AuNPs required a higher WETMM concentration (>0.2 mg mL^{-1}). In an attempt to obtain uncapped AuNPs, the WETMM concentration was further increased and AuNPs were obtained successfully at 0.8 mg mL^{-1} with a smaller particle size produced (86.4 ± 14.8 nm) than the capped AuNPs. In comparison to the AgNPs, uncapped AuNPs were much smaller than uncapped AgNPs synthesized using 0.1 mg mL^{-1} of WETMM. We have seen similar findings when higher concentration of extracts used.[29,30] However, there were also previous reports that showed the opposite relationship.[8,12] Thus, the role of WETMM concentration in influencing physical characteristics of formed NPs are currently not fully understood and warrants further investigation. In the current study, CS was mixed together into the reaction mixture as a one-pot production method. In the presence of CS during the reduction stage, AuNPs could be obtained even at lower concentrations (0.05–2.00 mg mL^{-1}) which further suggested that CS could play dual role as a stabilizer cum reducing agent in this formulation. Hence, WETMM concentration of 0.8 mg mL^{-1}, which was the minimum concentration to successfully synthesize AuNPs, was selected to produce uncapped formulations for AuNPs (F7). Uncapped AgNPs were synthesized using WETMM concentration of 0.1 mg mL^{-1} (F6). The PDI values for AgNPs and AuNPs were in the range of 0.22 ± 0.06 to 0.56 ± 0.03, indicating a moderate dispersity of particle sizes. Several formulations with the PDI values of 0.4 signifies their polydispesity,[31] probably due to the presence of aggregates in the formulations. Both uncapped AgNPs and AuNPs were respectively and when capped with CS, they had positive surface charges (+25.1 ± 0.37 to +37.3 ± 1.83 and +35.0 ± 8.46 to +40.5 ± 0.81 mV, respectively) due to the presence of protonated amino groups of CS coated onto the nanoparticle surfaces. Higher zeta potential values are desirable as the system is electrostatically stable because of repulsion between the particles.[12] On average, both capped AgNPs and AuNPs exhibited strong positive charge of ≥30 mV, indicating electrostatic stability of NPs provided by CS and hence, ensuring the particles were kept away from each other. These results suggested that CS was an efficient capping agent to stabilize the AgNPs, especially when paired with optimized concentration of reducing agent. Nevertheless, determination of long-term stability of these NPs is needed to determine the role of CS as a stabilizing agent.

XPS measurement

Fig. 3A shows the XPS spectrum of capped AgNPs in the range of 0–1200 eV. Wide scan demonstrated the presence of elements

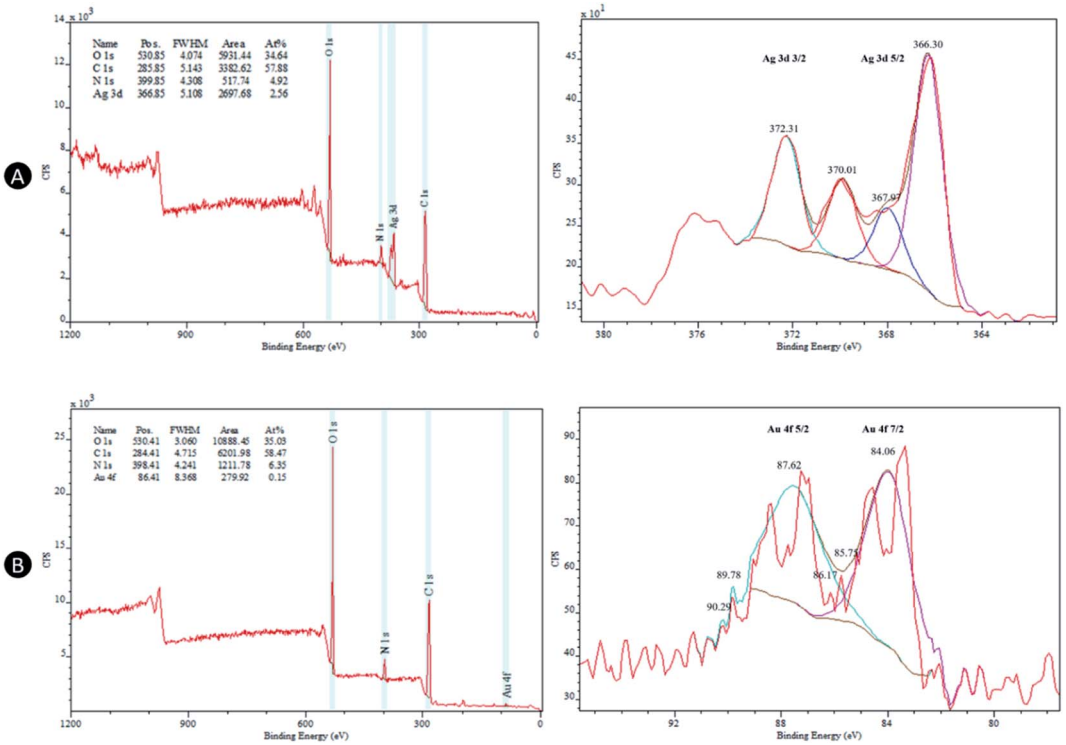

Fig. 3 Wide scan and high-resolution XPS spectra of (A) capped AgNPs and (B) capped AuNPs.

like oxygen (O 1s), nitrogen (N 1s), silver (Ag 3d) and carbon (C 1s). The doublet peak at spectrum region 363–380 eV is the characteristic of Ag 3d, whereas 531 eV, 286 eV and 400 eV are O 1s, C 1s and N 1s, respectively. The C 1s peak at 285.85 eV served as a reference to correct the binding shift.[32] The atomic percentages of O, C, N and Ag were also found to be 34.64%, 57.88%, 4.92% and 2.56%, respectively. Analysis of XPS spectrum on AgNPs sample confirms the presence of polymeric structure of CS (C 1s) as a capping agent of AgNPs, which prevents aggregation from occurring.

The two peaks at 367.97/366.30 eV and 372.31/370.01 eV in high-resolution XPS spectrum in Fig. 3A correspond to Ag 3d5/2 and Ag 3d3/2, respectively.[33] The peaks 372.31 eV and 367.97 eV represent metallic Ag, whereas 370.01 eV and 366.30 eV represent oxidized species of the Ag. NPs such as AgNPs exist in metastable state due to its nanoscale feature, which necessitates the employment of stabilizing agent to prevent growth of AgNPs. However, when exposed to air, some degree of metal oxide tends to form because Ag_2O is more thermodynamically favored under standard temperature and pressure conditions regardless of stabilizing agents.[34]

Similar patterns are seen in Fig. 3B except that Au 4f peak appears at position 86.41 eV in the AuNPs sample. The atomic percentages of O, C, N and Au were also found to be 35.03%, 58.47%, 6.35% and 0.15%, respectively. As for the high-resolution XPS spectrum in Fig. 3B, Au 4f are typically characterized by three pair of peaks, which occur due to the spin–orbit splitting of the Au 4f core level (Au 4f7/2 and Au 4f5/2).[35,36] Peaks at 84.06 eV and 87.62 eV correspond to metallic gold, whereas the smaller peaks shifted to the left of these pairs are related to two stable Au oxide species; Au^+ (85.75 eV and 89.78 eV) and Au^{3+} (86.17 eV and 90.29 eV).[37] As compared to Ag, Au are less easily oxidized which could explain lower intensity of these Au oxide states in relation to its metallic states.[34]

Morphology

Particle morphology was viewed under a TEM and the particle size distribution histograms of the samples were plotted to determine the mean diameters, standard deviation and polydispersity of nanoparticles. The morphology of AgNPs and AuNPs appeared to be spherical in shape as shown in TEM micrographs (Fig. 4A). Uncapped AgNPs were moderately dispersed, with significantly more aggregates present as compared to capped AgNPs. The particle size of uncapped AgNPs were in the range of 7.2–34.9 nm, much smaller than the particle size measured using DLS (200.9 ± 44.2 nm). The discrepancy is mainly because DLS is a more sensitive method that measures both large and small particles as well as aggregates in a solution, whereas TEM only measures single particles, which could contribute to biasness during sample preparation.[12] Aside from that, DLS computes hydrodynamic diameter of NPs including core and any particle attached on their surfaces.[38] The interaction between particles and dispersion media may also influence the hydrodynamic diameter.[21]

The AgNPs capped with CS were well dispersed with some degree of aggregation observed (Fig. 4B). This was validated by the higher standard deviation value as response to the particle size fluctuation as shown in the graph. A broad particle size

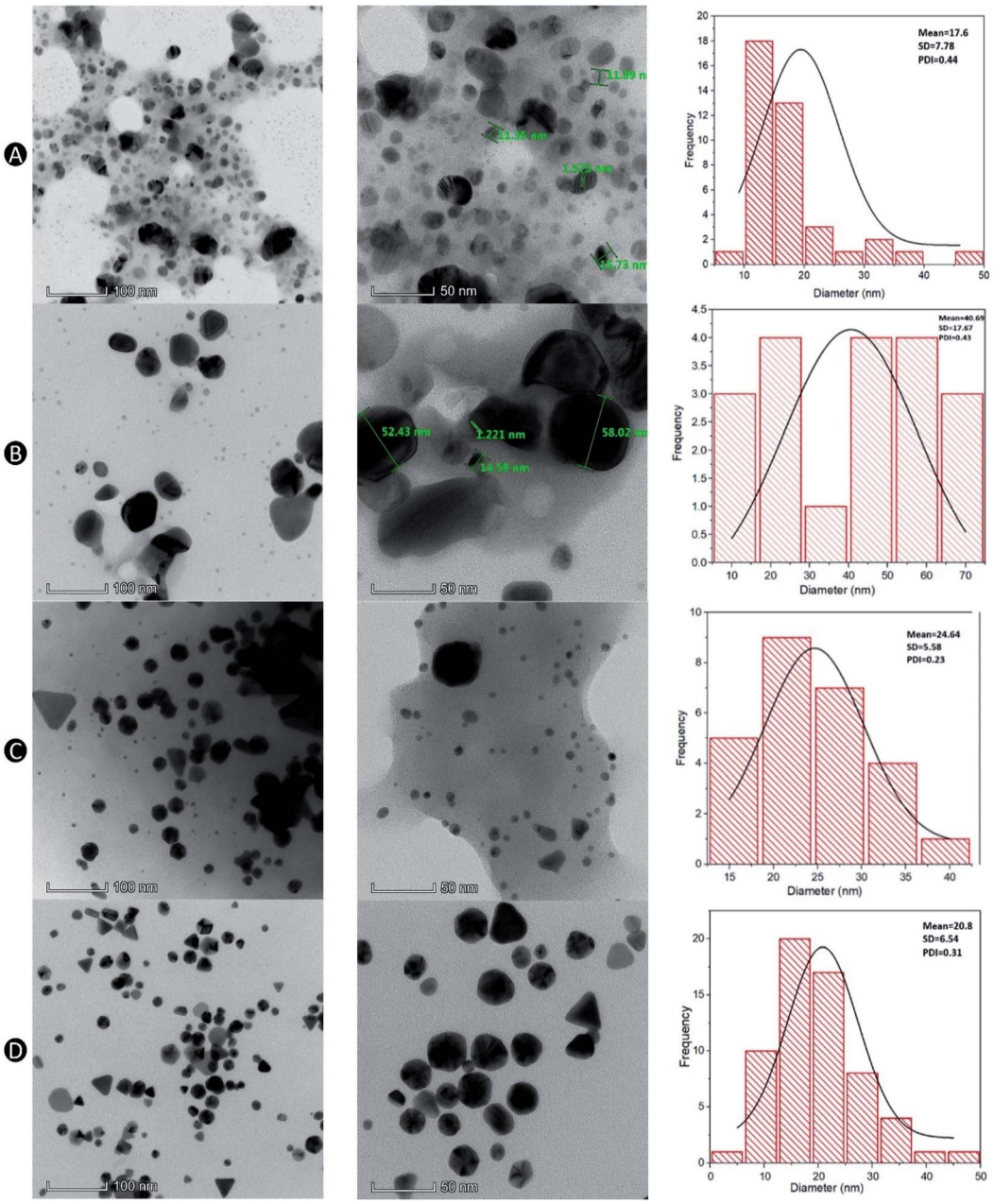

Fig. 4 TEM micrographs and their corresponding particle size distribution of (A) uncapped AgNPs and (B) capped AgNPs at 260 (left) and 600 kx (right) as well as (C) uncapped AuNPs and (D) capped AuNPs at 260 (left) and 600 kx (right).

distribution was observed regardless of the type of nanoparticle used, contributing to a greater PDI. In comparison to the PDI obtained from a Zetasizer provided in Table 2, all of the formulations with and without CS resulted in higher PDI except for uncapped AuNPs (0.40 ± 0.05). This is mainly due to an extra layer of solvent around the particles in the dispersed phase for the DLS method, which contributed to the larger particle sizes whereas smaller sizes of particles in dried state can be observed in the TEM micrographs.

The positive surface charge contributed by protonated amino groups in CS is responsible for the particle stability due to the repulsion between the particles. A possible explanation with regards to the presence of aggregates shown in the TEM micrographs is probably due to the flocculation between CS over time as the lyophilized samples were re-suspended in distilled water which therefore, less amino groups were protonated at higher pH than 5.9.[39] Although other samples in the TEM images shown smaller particle sizes, capped AgNPs exhibited particle size ranging from 6–58 nm, which is consistent with the results obtained using DLS method (58.4 ± 6.3 nm).

CS-stabilized AuNPs were generally spherical in shape with some triangle, rod and hexagon shaped NPs (Fig. 4C). In a different study, spherical and triangular nanoprism shaped

NPs were manufactured using chemical polyol method. However, more triangles were transformed from spherical NPs when the concentration of precursors were balanced.[40] Hence, the formation of these shapes might have been attributed to the concentration of WETMM (0.1 mg mL^{-1}) used in this study. The sizes in TEM micrographs for capped AuNPs were in the range of 8.9–32.1 nm. AuNPs without CS were generally smaller (6.7–39.5 nm) than the ones with CS (Fig. 4D), which supports previous report that this may have been attributed to the increased in hydrodynamic diameter to the size of inorganic core by CS as capping agent.[41]

FTIR analysis

FTIR is an analytical tool used to identify functional groups from the spectral bands of the compounds that are being tested.[42] In this study, it was conducted to study the possible chemical interaction and conjugation between WETMM and CS to synthesize the NPs. In a proteomic study of *Lignosus rhinocerotis*, the genome of the mushroom is largely prevalent of codes for polysaccharides such as 1,3-β- and 1,6-β-glucans and proteins.[9] Further analysis using liquid chromatography-mass spectrometry (LC-MS) revealed that polysaccharides and oligosaccharides were the main constituents of WETMM.[8] According to Fig. 4, the band at 3321.5 cm^{-1} for WETMM represents the C–H bending from aromatic hydrocarbons, broad O–H stretching from carboxylic group and phenol ring. The band at 1637.3 cm^{-1} corresponds to the C–OH alcohol group attached to benzene ring, C=O carbonyl group attached to alcohol, hydrocarbons and also amide I and amide II representing the proteins and aromatic amines. The subdued peak at 1280.7 cm^{-1} could correspond to C–O stretch on phenol ring or the C–O–C vibrations of carbohydrate of polysaccharides. The uncapped formulations of AgNPs and AuNPs spectra portrayed similar bands in Fig. 5.

This could mean that there were hydrogen bonds formed between the OH^- alcohol groups between WETMM and CS during the synthesis stage. AgNPs and AuNPs both had slight shift of bands from 3321.5 cm^{-1} to 3284.8 cm^{-1} (AgNPs) and 3295.8 cm^{-1} (AuNPs) which could mean that there was involvement of this hydroxyl functional group during the reduction period.[8] Oxidation process of the hydroxyl groups from polysaccharides, proteins and oligosaccharides forms carbonyl, which in turn facilitates the formation of AgNPs from its ionic state.[8] Reducing sugar from WETMM also has free

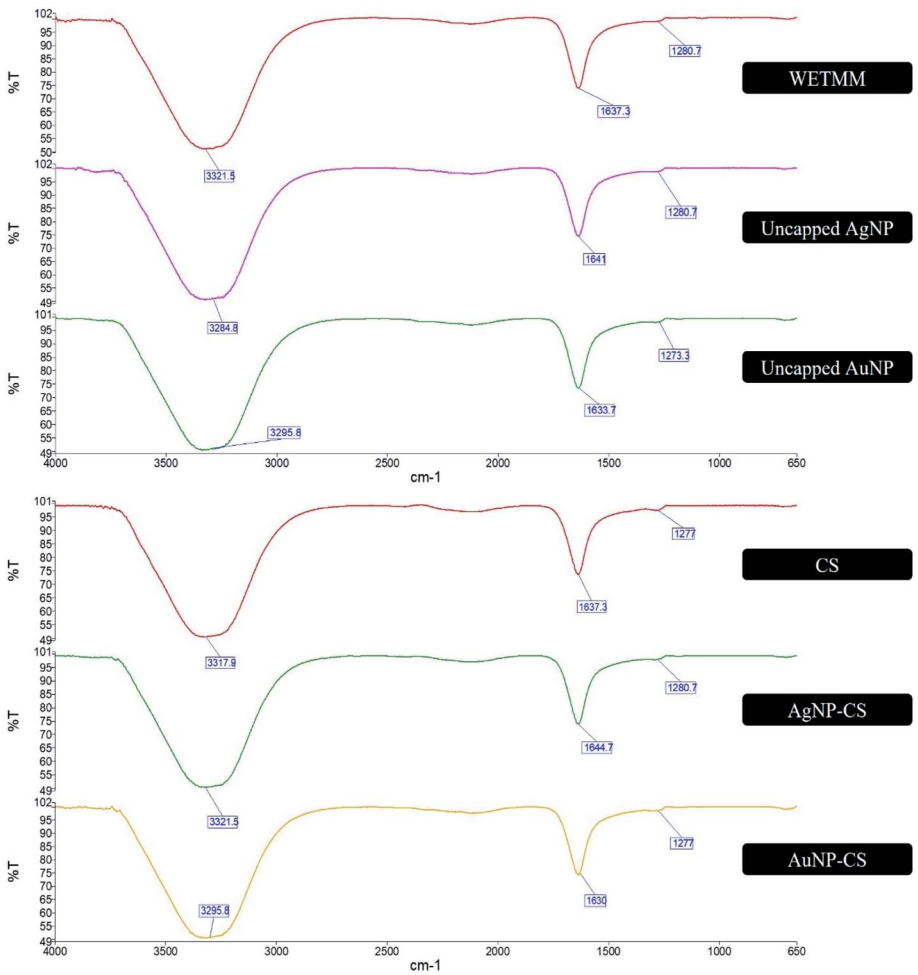

Fig. 5 FTIR spectra of WETMM, uncapped AgNPs, uncapped AuNPs, CS, capped AgNPs and capped AuNPs.

aldehyde groups of the hemiacetalic hydroxyl group to serve as electron donor to reduce these metal ions into 0 oxidation state.[19]

As for the spectra of CS, the broad band at 3317.9 cm^{-1} represents the aromatic C–H compounds and O–H stretching attached to the aromatic hydrocarbon and alkane. This peak overlaps with the N–H amide stretch attached to the benzene ring, which is also usually present at 3300–3500 cm^{-1} region. Band at 1637.3 cm^{-1} corresponds to C=O (amide I) and amide II (N–H) of CS.[23] It could also be due to the carbonyl stretch vibrations in ketones, aldehydes and carboxylic acids, showing that the reduction of silver ions is coupled to the oxidation of the hydroxyl groups in the CS molecule or its hydrolyzates.[43] This finding supports the earlier discussion that the immediate presence of CS during reduction stage could enhance reducing capacities, which resulted in more AgNPs being formed with less lingering Ag^+. The band at 1277 cm^{-1} represents the primary amine group C–N–H_2 and C–O–C bridge of CS. The formation of C–O–C bridge could be due to the formation self-assembled monolayer encircling AgNPs and AuNPs as proposed by a report on the interaction between CS and AgNPs as its stabilizing agent.[8] Variation in positions of the peaks for AgNPs and AuNPs compared to pure CS at the 3300 cm^{-1} (OH^- and NH_2) region could be due to the contribution of CS during reduction and stabilization process.[20] In summary, FTIR spectra in Fig. 4 demonstrated that AgNPs and AuNPs biosynthesis were aided by reduction capacities of both CS and WETMM and successfully capped by CS for nanoparticle stability.

Antibacterial activity

In this study, well established and universally accepted methods of agar well diffusion and microbroth dilution were employed to investigate the antibacterial effect of uncapped and capped AgNPs and AuNPs against Gram-positive (*S. aureus*) and -negative (*P. aeruginosa*) bacteria. In the microbroth dilution method, ciprofloxacin HCl was used as positive control. Both MIC and zone of inhibition values of ciprofloxacin HCl against *S. aureus* (ATCC 25923; 32–38 mm) and *P. aeruginosa* (ATCC 27853; $\leq$0.5 μg mL^{-1}) were well within the quality control range of Clinical & Laboratory Standards Institute (CLSI).[44,45] TTC reagent was used to evaluate the antibacterial activity of AgNPs and AuNPs as it can detect and stain live bacteria at fewer bacterial counts.[46] Formulation F4 of both AgNPs and AuNPs were selected for *in vitro* evaluation of antibacterial activity owing to their acceptable physical characteristics and faster NP formation.

According to Fig. 6, all of the samples appeared to have antibacterial effects against both Gram-positive and -negative strains, albeit generally AgNPs were much superior as opposed to the AuNPs counterpart. The mode of action of AgNPs against bacteria are multiple.[18] In this nanoparticle state, they can accumulate along the trenches on the cell wall after they have attached themselves on the surface and penetrate bacterial cell walls due to its nanoscale size. Once inside the cells, the NPs wreak havoc by damaging cell organelles, resulting in cell lysis. Other than that, AgNPs can also disrupt signal transduction within the cell *via* dephosphorylation of tyrosine residues on the peptide substrates. This process is important for bacterial signal transduction. On the other hand, AgNPs can continually release Ag^+ which is toxic to bacteria. Outside the cell, ions that are adhered to the cell wall and membrane can enhance permeability of the cytoplasmic membrane to increase uptake of both AgNPs and Ag^+. Within the cell, Ag^+ can deactivate respiratory enzymes and generate reactive oxygen species by interrupting adenosine triphosphate (ATP) production.[18]

Although it is widely reported that AgNPs have more activity against Gram-negative bacteria due to its narrow cell wall and negatively charged lipopolysaccharides,[12,18,22] AgNPs biosynthesized by using WETMM in this study had resulted in lower MIC values against *S. aureus*, indicating a better activity against Gram-positive bacteria. These MIC values are similar to AgNPs biosynthesized using mushroom waste of *Pleurotus ostreatus* and stabilized by CS against Gram-positive (*S. aureus* ATCC 6538 and *Bacillus* sp. ATCC 27380) and Gram-negative (*P. aeruginosa* ATCC 9027 and *E. coli* ATCC 25927) despite the jarring difference in their particle sizes (281 $\pm$ 6 nm).[21] Perhaps the difference between the particle sizes were not significant enough to influence its inhibitory properties against the tested microbes at concentration 5 $\times$ 10^5 CFU mL^{-1} during the antibacterial assay. In general, nanoparticle size of less than 50 nm is well accepted for optimum cellular uptake,[47,48] explaining similar antibacterial activity of both AgNPs with different particle sizes. With regards to the lower MIC value for *S. aureus* demonstrated in current study, one of the explanations could be due to the antimicrobial property of CS.[12,49] The antibacterial mechanism of CS is not fully understood but it is hypothesized that it can interact with the charged cell membrane surface, facilitating the penetration into phospholipid bilayer and disrupting the cytoplasmic membrane.[23] Another possibility that could explain the superior efficacy against *S. aureus* is the use of WETMM as the reducing agent that also exhibits antimicrobial property.[9] *In vitro* study showed that both methanol and WETMM at 30 mg mL^{-1} could significantly inhibit against various microbes due to the presence of alkaloids, protein, gums, mucilage and flavonoids. Out of the 19 microbes tested, WETMM had demonstrated the highest zone of inhibition against *S. aureus*.[10]

Interestingly, the CS-stabilized AgNPs had higher MIC values than the uncapped AgNPs. Similar findings were observed for AgNPs biosynthesized using mushroom waste of *Pleurotus ostreatus*. It was probably due to the CS coat that acted as an additional barrier, whereas uncapped AgNPs can act directly against the bacteria.[21] Moreover, it could also be due to the formulation of AgNPs itself. The biosynthesis method involved mixing of WETMM, $AgNO_3$ and CS at a ratio of 5 : 1 : 5, whereas uncapped AgNPs were only synthesized using WETMM and $AgNO_3$ at a ratio of 5 : 1. The addition of CS into the formula further diluted the molar concentration of silver, which could have affected its overall antibacterial efficacy. In this case, MIC of CS-stabilized AgNPs were higher by 1 dilution level (two-fold) *versus* uncapped AgNPs which is approximately similar to the two-fold dilution of molar concentration of silver during the synthesis stage.

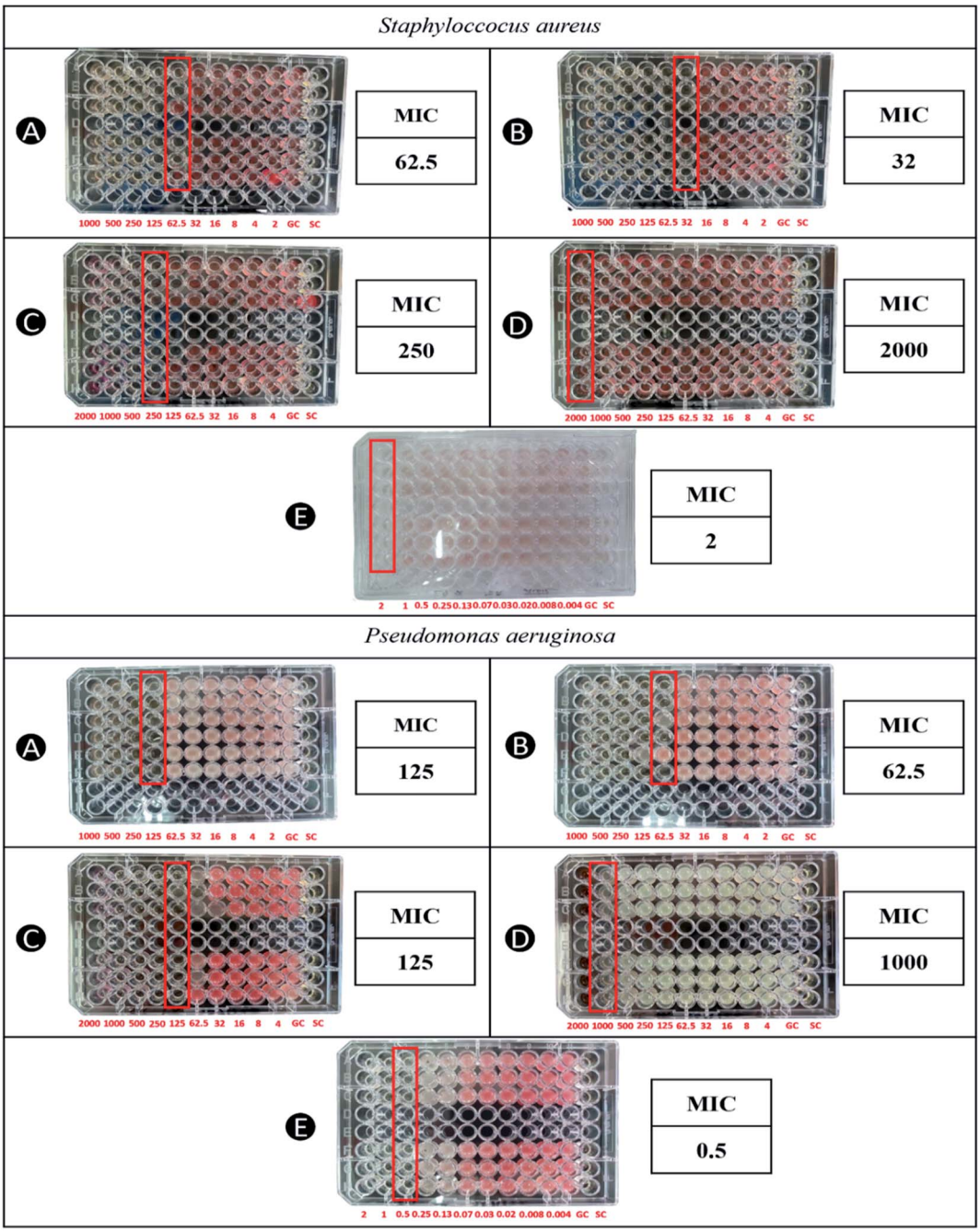

Fig. 6 MIC of (A) capped AgNPs, (B) uncapped AgNPs, (C) capped AuNPs, (D) uncapped AuNPs, and (E) ciprofloxacin HCl against *S. aureus* and *P. aeruginosa* as determined by microbroth dilution assay.

The MIC values obtained for AuNPs against *P. aeruginosa* and *S. aureus* strains were 125 and 250 μg mL^{-1}, respectively. Based on this result, AuNPs demonstrated better antimicrobial activity on *P. aeruginosa* compared to *S. aureus*. Gram-positive bacteria have a strong cell wall that hinders foreign intrusion, whereas Gram-negative bacteria have a thin cell wall that allows AuNPs to enter the cell membrane.[50] The antibacterial mechanism of AuNPs is mostly similar to AgNPs. They work by binding to the surface of bacteria, creating pits and holes that lead to the leakage of the cell contents, inflicting considerable damage to the membrane and DNA and perhaps leading to cell death.[51,52] Uncapped AuNPs had shown a weak antibacterial activity. However, CS-stabilized AuNPs possess better antimicrobial effect, most probably due to the CS coating.[53] CS stabilization on AuNPs contributes high positive surface charge causing strong adhesion to the cell wall. This is due to the interaction between protonated NH^{3+} groups of CS and negatively charged microbial cell.[54]

Interestingly, AgNPs displayed opposite effect to AuNPs whereby the formulation without CS had lower MIC values than

Table 3 Zone of inhibition *S. aureus* and *P. aeruginosa* for the biosynthesized AgNPs and AuNPs, $n = 3$

	Zone of inhibition (mm)	
Samples	*S. aureus*	*P. aeruginosa*
Ciprofloxacin (20 μg mL^{-1})	31.7 ± 2.9	23 ± 3.6
Ciprofloxacin disc (5 μg)	31.3 ± 0.6	—
CS (0.09% w/v)	—	—
AgNPs (1 mg mL^{-1})	14.3 ± 2.7	13.3 ± 1.5
AgNP-CS (1 mg mL^{-1})	11.7 ± 1.5	8.3 ± 0.6
AuNPs (1 mg mL^{-1})	—	—
AuNP-CS (1 mg mL^{-1})	5.7 ± 1.2	6.1 ± 0.2

CS-stabilized AgNPs. One possibility to this occurrence is that CS might have interacted differently with AuNPs, which could also explain the reason why the particle sizes of AuNPs were mostly larger with CS attachment than without. Further tests are needed as FTIR analysis alone was not able to distinguish between these interactions. Zones of inhibition from agar well diffusion assay are presented in Table 3. In this test, capped AgNPs and AuNPs demonstrated activity against both *P. aeruginosa* and *S. aureus*, whereas without CS, only uncapped AgNPs formulation was able to inhibit the growth of bacteria. Inhibition zones of capped AgNPs were lower than uncapped AgNPs for both Gram-positive and -negative bacteria. AgNPs also formed larger zones of inhibition towards *S. aureus* than *P. aeruginosa*. These findings are consistent with the MIC values determined from the microbroth dilution method.

As for the AuNPs, inhibition zones against *P. aeruginosa* were higher than *S. aureus*, corroborating to their superior efficacy towards Gram-negative bacteria. Antibacterial activity of CS was also tested as a control, indicating that the zone of inhibitions formed by AuNPs stabilized by CS were indeed caused by the AuNP–CS complex and not by CS. Although there are reports that demonstrated antimicrobial activity of CS, the concentration used in this study is much lower. It is also important to note that CS activity against bacteria could vary depending on its deacetylation degree and molecular weight.[55] However, AuNPs formulation without CS had shown no antibacterial activity against both bacteria. Evidence suggests that bare AuNPs have no effect on bacterial growth when tested using agar well diffusion, whereas conjugated AuNPs with biomolecules decrease bacterial growth.[41] In this case, absence of antibacterial activity could also be attributed to the high concentration of WETMM (0.8 mg mL^{-1}) used to synthesize AuNPs without CS. In previous study, inhibition zones of *S. aureus* and *P. aeruginosa* were decreased when WETMM concentration was increased from 0.0125 to 0.05 mg mL^{-1}.[8] When AuNPs were stabilized using CS, increasing concentration of CS formed larger diameter of inhibition zones,[8] which is a proof that CS is an important component in this formulation to facilitate antibacterial activity for AuNPs.

Anti-biofilm potential

There are many tests used for anti-biofilm assay such as the qualitative tube method, of which biofilm formation is determined by observing the thin layer of blue film on walls of tube[56] and the qualitative Congo red agar method, which observes black crystalline colonies on the agar indicating formation of EPS production.[57] However, the microtiter plate assay was used to quantitatively estimate the biofilm growth. *S. aureus* and *P. aeruginosa* were selected as test microbes because they are well-known biofilm formers.[58] Susceptibility to AgNPs and AuNPs on biofilm growth is highly strain dependent.[59] According to Table 4, biofilm inhibition of AuNPs and AgNPs were both higher without CS in formulation against *S. aureus*. In an *in vitro* study using low molecular weight (MW) CS, biofilm formation was reportedly increased at sub-bacteriostatic (0.003% w/v) concentration. It was probably due to the stress response mechanism of the bacteria against CS.[39] In another study, different antibiotics and NaCl demonstrated increased biofilm growth at toxic concentrations, which was partially due to heightened expression of polysaccharide intercellular adhesin (PIA). PIA is a component of biofilm matrix.[60] This could explain why NPs without CS were superior in biofilm inhibition *versus* CS-stabilized AgNPs and AuNPs (capped NPs) as the anti-biofilm effect was off-set by CS in the latter formulation. By comparison, activity against biofilm formation using AgNPs produced by chemical reduction method was as high as 74–86% at 100 μg mL^{-1}. In this study, AgNPs at MIC values (125 μg mL^{-1} for *P. aeruginosa*; 62.5 μg mL^{-1} for *S. aureus*) managed to inhibit biofilm formation by 53.21% (*P. aeruginosa*) and 46.24% (*S. aureus*). One of the reasons could be due to the particle size of the NPs formed. Particles larger than 50 nm are difficult to enter biofilm due to its complicated architecture,[18] which reinforces the importance of synthesizing small NPs at production stage

Table 4 Biofilm inhibition against *S. aureus* and *P. aeruginosa* for AgNPs, AgNP-CS, AuNPs, AuNP-CS and ciprofloxacin at MIC, $n = 3$

	Bacteria			
Samples	Conc. (μg mL^{-1})	*S. aureus* (%)	Conc. (μg mL^{-1})	*P. aeruginosa* (%)
AgNPs	32	64.64 ± 15.47	62.5	46.24 ± 18.48
AgNP-CS	62.5	48.71 ± 3.83	125	53.21 ± 11.00
AuNPs	1000	73.04 ± 1.73	1000	54.11 ± 16.21
AuNP-CS	250	48.16 ± 27.95	125	79.39 ± 2.45[a]
Positive control (ciprofloxacin)	2	77.37 ± 2.89	0.5	43.78 ± 5.93

[a] Statistically different from the positive control ($p < 0.05$); conc. – concentration.

for better anti-biofilm effect. Although the biofilm inhibition of all the formulations were lower than the positive control, they were considered comparable as the differences were statistically insignificant ($p > 0.05$).

On the other hand, both CS-stabilized AuNPs and AgNPs (capped NPs) appeared to have higher biofilm inhibition against *P. aeruginosa* compared to *S. aureus*. Similar findings were observed elsewhere for AgNPs in combination with CS[21] and CS alone.[61] Cell wall gram type does not play a role in difference between the responses, rather it was due the type of matrix. Gram-negative bacteria such as *P. aeruginosa* have thick matrix, which makes them highly susceptible to CS. Some exopolysaccharides (EPS), which is a component of biofilm, from *P. aeruginosa* are known to be polyanionic whereas *S. aureus* are polycationic. Hence, penetration into the matrix could have been facilitated by CS due to its positive charges.[60]

Higher concentrations and deacetylation degrees (DD) of CS affect the stability of AgNP–CS complexes and determine the positive charge and solubility of CS. More than 65% of DD is needed to achieve stable complexation. However, DD of CS as high as more than 85% had shown blood incompatibilities in *in vivo* studies and many other non-specific effects due to large free excess of cationic CS.[62] Thus, 75% of CS was used in this work. Higher DD is also good for cell interactions. As stated earlier, EPS from *Pseudomonas* sp. are known to be polyanionic in nature. Hence, penetration into the matrix could depend on the positive charge and size of CS.[61] As for the MW of CS, a lower MW is usually much preferred as it can produce smaller sizes of nanoparticles. Particles larger than 50 nm are generally difficult to enter the biofilm.[18] Even so, there needs to be a balance in the MW of CS because a higher MW will form stable complexes and prevent aggregation to occur between the AgNPs. In a report, optimum MW of CS is 65–170 kDa, which is well within the range of CS MW used in this study.[62] Optimum concentration of CS needed to generate anti-biofilm effects are still inconclusive as there are many contradicting reports, which leads to the possibility that the anti-biofilm effects are strain dependent. AgNPs drew similar resemblance as many other researchers concluded that its anti-biofilm effects were also strain dependent.[59] A study also stated that high percentage of reduction in the biofilm production by *P. aeruginosa* is linked to disruption of the EPS matrix caused by the NPs.[63] In general, both formulations of AuNPs registered higher biofilm inhibition when compared to their silver counterparts. CS-stabilized AuNPs reduce biofilm development by *P. aeruginosa* by 79.39% and *S. aureus* by 48.16%. This could be due to the higher surface charge of AuNPs ($+35.7 \pm 4.51$) *versus* the AgNPs ($+31.7 \pm 4.80$), which is important in attachment to the EPS of biofilm. Out of all the formulations, only the biofilm inhibition by capped AuNPs were statistically different from the positive control ($p < 0.05$), showing a significant enhanced anti-biofilm activity.

Although there are many reports that attribute AgNPs and AuNPs to their anti-biofilm property, there are also many other works that demonstrated underwhelming inhibitory effect on biofilm, especially when the NPs were synthesized biologically.[12,21] In this case, CS concentration could have been reduced to subdue the negative anti-biofilm effect or the NPs could be conjugated with other substance with established anti-biofilm property to improve the overall formulation such as lactoferrin[12].

Conclusion

In this study, WETMM had successfully reduced AgNPs and AuNPs and CS as the stabilizing agent could prevent aggregation of both NPs. The fabricated NPs were within 200 nm in particle sizes with the smallest recorded was 58.4 ± 6.3 nm. TEM micrographs show that they were mostly spherical, with some triangular nanoprisms observed for AuNPs. Both AuNPs and AgNPs demonstrated an antibacterial activity against *S. aureus* and *P. aeruginosa* and the presence of CS did not show a clear trend in the antimicrobial enhancement activities. This warrants further investigation on the interaction between CS and the heavy metals. The anti-biofilm effect of CS-stabilized AuNPs and AgNPs were much higher against *P. aeruginosa* compared to *S. aureus* but, in general the anti-biofilm activity was comparable to the positive control except for CS-stabilized AuNPs that exhibited a significant enhanced activity. There were many rooms for improvements in terms of optimizing the NPs produced and enhancing the anti-biofilm activities, however these findings provide further understanding and knowledge on biosynthesizing NPs using WETMM and stabilizing with CS. Overall, this study opens a lot more interesting avenues for research to enhance and promote the application of bionanoparticles for treating infections of chronic wounds.

Conflicts of interest

There are no conflicts to declare. The authors alone are responsible for the content and writing of this article.

Acknowledgements

This study is financially supported by Geran Arus Perdana, Universiti Kebangsaan Malaysia (GUP-2019-004).

Notes and references

1 B. Mubeen, A. N. Ansar, R. Rasool, I. Ullah, S. S. Imam, S. Alshehri, *et al.*, Nanotechnology as a Novel Approach in Combating Microbes Providing an Alternative to Antibiotics, *Antibiotics*, 2021, **10**(12), 1473.

2 J. L. Clement and P. S. Jarrett, Antibacterial Silver, *Metal-Based Drugs*, 1994, **1**(5–6), 467–482.

3 S. S. I. Abdalla, H. Katas, F. Azmi and M. F. M. Busra, Antibacterial and Anti-Biofilm Biosynthesised Silver and Gold Nanoparticles for Medical Applications: Mechanism of Action, Toxicity and Current Status, *Curr. Drug Deliv.*, 2019, **17**(2), 88–100.

4 P. Taylor, M. C. Ammons and V. Copié, Mini-review: lactoferrin: a bioinspired, anti-biofilm therapeutic, *J. Bioadhes. Biofilm Res.*, 2013, 37–41.

5 K. Kalishwaralal, S. BarathManiKanth, S. R. K. Pandian, V. Deepak and S. Gurunathan, Silver nanoparticles impede

the biofilm formation by Pseudomonas aeruginosa and Staphylococcus epidermidis, *Colloids Surf. B Biointerfaces*, 2010, **79**(2), 340–344.
6 S. Horikoshi and N. Serpone, Introduction to Nanoparticles, *Microwaves in Nanoparticle Synthesis: Fundamentals and Applications*, 2013, vol. 1–24.
7 S. Prabhu and E. K. Poulose, Silver nanoparticles: synthesis, mechanism of antimicrobial action, characterization, medical applications, and toxicity effects, *J. Chem. Pharmaceut. Res.*, 2016, **8**(2), 526–537.
8 H. Katas, C. S. Lim, A. Y. H. Nor Azlan, F. Buang and M. F. Mh Busra, Antibacterial activity of biosynthesized gold nanoparticles using biomolecules from Lignosus rhinocerotis and chitosan, *Saudi Pharmaceut. J.*, 2019, **27**(2), 283–292, DOI: **10.1016/j.jsps.2018.11.010**.
9 N. Nallathamby, C. W. Phan, S. L. S. Seow, A. Baskaran, H. Lakshmanan, S. N. Abd Malek, *et al.*, A status review of the bioactive activities of tiger milk mushroom Lignosus rhinocerotis (Cooke) Ryvarden, *Front. Pharmacol.*, 2018, **8**, DOI: **10.3389/fphar.2017.00998**.
10 S. Mohanarji, S. Dharmalingam, A. Kalusalingam and A. Science, Screening of Lignosus rhinocerus Extracts as Antimicrobial Agents against Selected Human Pathogens, *J. Pharmaceut. Biomed. Sci.*, 2012, **18**(18), 1–4.
11 S. Govindan, E. A. K. Nivethaa, R. Saravanan, V. Narayanan and A. Stephen, Synthesis and characterization of chitosan–silver nanocomposite, *Appl. Nanosci.*, 2012, **2**(3), 299–303.
12 S. Abdalla, H. Katas, J. Y. Chan, P. Ganasan, F. Azmi and M. Fauzi Mh Busra, Antimicrobial activity of multifaceted lactoferrin or graphene oxide functionalized silver nanocomposites biosynthesized using mushroom waste and chitosan, *RSC Adv.*, 2020, **10**(9), 4969–4983.
13 A. Y. H. Nor Azlan, H. Katas, N. H. Habideen and M. F. Mh Busra, Dual-action of thermoresponsive gels containing DsiRNA-loaded gold nanoparticles for diabetic wound therapy: characterization, in vitro safety and healing efficacy, *Saudi Pharmaceut. J.*, 2020, **28**(11), 1420–1430, DOI: **10.1016/j.jsps.2020.09.007**.
14 M. M. S. M. Sabee, M. S. Awang, Y. Bustami and Z. A. A. Hamid, Gentamicin loaded PLA microspheres susceptibility against staphylococcus aureus and escherichia coli by kirby-bauer and micro-dilution methods, in *AIP Conference Proceedings*, American Institute of Physics Inc., 2020.
15 I. Wiegand, K. Hilpert and R. E. W. Hancock, Agar and broth dilution methods to determine the minimal inhibitory concentration (MIC) of antimicrobial substances, *Nat. Protoc.*, 2008, **3**(2), 163–175.
16 M. Sandasi, C. M. Leonard and A. M. Viljoen, The effect of five common essential oil components on Listeria monocytogenes biofilms, *Food Control*, 2008, **19**(11), 1070–1075.
17 I. M. Famuyide, A. O. Aro, F. O. Fasina, J. N. Eloff and L. J. McGaw, Antibacterial and antibiofilm activity of acetone leaf extracts of nine under-investigated south African Eugenia and Syzygium (Myrtaceae) species and their selectivity indices, *BMC Compl. Alternative Med.*, 2019, **19**(1), 141.
18 I. X. Yin, J. Zhang, I. S. Zhao, M. L. Mei, Q. Li and C. H. Chu, The antibacterial mechanism of silver nanoparticles and its application in dentistry, *Int. J. Nanomed.*, 2020, **15**, 2555–2562.
19 N. Vigneshwaran, A. A. Kathe, P. v. Varadarajan, R. P. Nachane and R. H. Balasubramanya, Silver-protein (core-shell) nanoparticle production using spent mushroom substrate, *Langmuir*, 2007, **23**(13), 7113–7117.
20 M. Venkatesham, D. Ayodhya, A. Madhusudhan, N. Veera Babu and G. Veerabhadram, A novel green one-step synthesis of silver nanoparticles using chitosan: catalytic activity and antimicrobial studies, *Appl. Nanosci*, 2014, **4**(1), 113–119.
21 H. Katas, M. A. Mohd Akhmar and S. Suleman Ismail Abdalla, Biosynthesized silver nanoparticles loaded in gelatine hydrogel for a natural antibacterial and anti-biofilm wound dressing, *J. Bioact. Compat Polym.*, 2021, **36**(2), 111–123.
22 J. S. Kim, E. Kuk, K. N. Yu, J. H. Kim, S. J. Park, H. J. Lee, *et al.*, Antimicrobial effects of silver nanoparticles, *Nanomed.: Nanotechnol. Biol. Med.*, 2007, **3**(1), 95–101.
23 S. Kumar-Krishnan, E. Prokhorov, M. Hernández-Iturriaga, J. D. Mota-Morales, M. Vázquez-Lepe, Y. Kovalenko, *et al.*, Chitosan/silver nanocomposites: synergistic antibacterial action of silver nanoparticles and silver ions, *Eur. Polym. J.*, 2015, **67**, 242–251.
24 P. Abrica-González, J. A. Zamora-Justo, A. Sotelo-López, G. R. Vázquez-Martínez, J. A. Balderas-López, A. Muñoz-Diosdado, *et al.*, Gold nanoparticles with chitosan, N-acylated chitosan, and chitosan oligosaccharide as DNA carriers, *Nanoscale Res. Lett.*, 2019, **14**(1), 258.
25 F. J. Flórez Barajas, Z. C. Sánchez Acevedo and H. Peña Pedraza, Synthesis and characterization of gold nanoparticles in solution using chitosan as reducing agent, *Respuestas*, 2019, **24**(2), 49–55.
26 M. G. Fuster, M. G. Montalbán, G. Carissimi, B. Lima, G. E. Feresin, M. Cano, *et al.*, *Antibacterial Effect of Chitosan-Gold Nanoparticles and Computational Modeling of the Interaction between Chitosan and a Lipid Bilayer Model*, available from: **https://www.mdpi.com/journal/nanomaterials**.
27 Y. K. Twu, Y. W. Chen and C. M. Shih, Preparation of silver nanoparticles using chitosan suspensions, *Powder Technol.*, 2008, **185**(3), 251–257.
28 M. A. G. Raja, H. Katas and T. J. Wen, Stability, intracellular delivery, and release of siRNA from chitosan nanoparticles using different cross-linkers, *PLoS One*, 2015, **10**(6), e0128963.
29 J. Y. Song, H. K. Jang and B. S. Kim, Biological synthesis of gold nanoparticles using Magnolia kobus and Diopyros kaki leaf extracts, *Process Biochem.*, 2009, **44**(10), 1133–1138.
30 S. Iravani, Green synthesis of metal nanoparticles using plants, *Green Chem.*, 2011, **13**(10), 2638–2650.
31 S. Bhattacharjee, DLS and zeta potential - What they are and what they are not?, *J. Controlled Release*, 2016, **235**, 337–351.

32 B. Ajitha, Y. Ashok Kumar Reddy and P. Sreedhara Reddy, Green synthesis and characterization of silver nanoparticles using Lantana camara leaf extract, *Mater. Sci. Eng. C*, 2015, **49**, 373–381.

33 J. Ruíz-Baltazar Á de, S. Y. Reyes-López, M. d. L. Mondragón-Sánchez, M. Estevez, A. R. Hernández-Martinez and R. Pérez, Biosynthesis of Ag nanoparticles using Cynara cardunculus leaf extract: evaluation of their antibacterial and electrochemical activity, *Results Phys.*, 2018, **11**, 1142–1149.

34 H. T. Phan and A. J. Haes, What Does Nanoparticle Stability Mean? Vol. 123, *J. Phys. Chem. C*, 2019, 16495–16507.

35 J. P. Sylvestre, A. v. Kabashin, E. Sacher, M. Meunier and J. H. T. Luong, Nanoparticle size reduction during laser ablation in aqueous solutions of cyclodextrins, in *Photon Processing in Microelectronics and Photonics III*, SPIE, 2004, p. 84.

36 D. K. Božanić, A. S. Luyt, L. v. Trandafilović and V. Djoković, Glycogen and gold nanoparticle bioconjugates: controlled plasmon resonance via glycogen-induced nanoparticle aggregation, *RSC Adv.*, 2013, **3**(23), 8705–8713.

37 J. P. Sylvestre, S. Poulin, A. v. Kabashin, E. Sacher, M. Meunier and J. H. T. Luong, Surface chemistry of gold nanoparticles produced by laser ablation in aqueous media, *J. Phys. Chem. B*, 2004, **108**(43), 16864–16869.

38 H. Fissan, S. Ristig, H. Kaminski, C. Asbach and M. Epple, Comparison of different characterization methods for nanoparticle dispersions before and after aerosolization, *Anal. Methods*, 2014, **6**(18), 7324–7334.

39 I. S. Dragland, H. V. Rukke, I. S. R. Stenhagen, J. Lönn-Stensrud and H. M. Kopperud, Antibacterial and Antibiofilm Effect of Low Viscosity Chitosan against Staphylococcus epidermidis, *Int. J. Microbiol.*, 2016, **2016**, 9159761.

40 B. Khodashenas and H. R. Ghorbani, Synthesis of silver nanoparticles with different shapes, *Arab. J. Chem.*, 2019, **12**(8), 1823–1838, DOI: **10.1016/j.arabjc.2014.12.014**.

41 G. L. Burygin, B. N. Khlebtsov, A. N. Shantrokha, L. A. Dykman, V. A. Bogatyrev and N. G. Khlebtsov, On the enhanced antibacterial activity of antibiotics mixed with gold nanoparticles, *Nanoscale Res. Lett.*, 2009, **4**(8), 794–801.

42 K. Torres-Rivero, J. Bastos-Arrieta, N. Fiol and A. Florido, Metal and metal oxide nanoparticles: an integrated perspective of the green synthesis methods by natural products and waste valorization: applications and challenges, in *Comprehensive Analytical Chemistry*, Elsevier B.V., 2021, pp. 433–69.

43 D. Wei, W. Sun, W. Qian, Y. Ye and X. Ma, The synthesis of chitosan-based silver nanoparticles and their antibacterial activity, *Carbohydr. Res.*, 2009, **344**(17), 2375–2382.

44 CLSI, *Performance Standards for Antimicrobial Susceptibility Testing, CLSI supplement M100*, PA: Clinical and Laboratory Standards Institute, Wayne, 30th edn, 2020.

45 J. E. Ross, L. C. Liverman and R. N. Jones, Determination of disk diffusion and MIC quality control guidelines for JNJ-Q2, a novel quinolone, *J. Clin. Microbiol.*, 2011, **49**(8), 3009–3011.

46 S. H. Moussa, A. A. Tayel, A. A. Al-Hassan and A. Farouk, Tetrazolium/Formazan Test as an Efficient Method to Determine Fungal Chitosan Antimicrobial Activity, *J. Mycol.*, 2013, **2013**, 1–7.

47 J. R. Morones, J. L. Elechiguerra, A. Camacho, K. Holt, J. B. Kouri, J. T. Ramírez, *et al.*, The bactericidal effect of silver nanoparticles, *Nanotechnology*, 2005, **16**(10), 2346–2353.

48 R. Itani and A. Faraj, SiRNA conjugated nanoparticles—a next generation strategy to treat lung cancer, *Int. J. Mol. Sci.*, 2019, **20**(23), 6088.

49 M. E. I. Badawy, T. M. R. Lotfy and S. M. S. Shawir, Preparation and antibacterial activity of chitosan-silver nanoparticles for application in preservation of minced meat, *Bull. Natl. Res. Cent.*, 2019, **43**(1), 83.

50 S. A. Akintelu, B. Yao and A. S. Folorunso, Green Synthesis, Characterization, and Antibacterial Investigation of Synthesized Gold Nanoparticles (AuNPs) from Garcinia kola Pulp Extract, *Plasmonics*, 2021, **16**(1), 157–165.

51 H. Katas, N. Z. Moden, C. S. Lim, T. Celesistinus, J. Y. Chan, P. Ganasan, *et al.*, Biosynthesis and Potential Applications of Silver and Gold Nanoparticles and Their Chitosan-Based Nanocomposites in Nanomedicine, *J. Nanotechnol.*, 2018, **2018**.

52 R. Imani, S. H. Emami, P. R. Moshtagh, N. Baheiraei and A. M. Sharifi, Preparation and characterization of agarose-gelatin blend hydrogels as a cell encapsulation matrix: an in-vitro study, *J. Macromol. Sci., Part B: Phys.*, 2012, **51**(8), 1606–1616.

53 J. Gouyau, R. E. Duval, A. Boudier and E. Lamouroux, Investigation of nanoparticle metallic core antibacterial activity: gold and silver nanoparticles against Escherichia coli and Staphylococcus aureus, *Int. J. Mol. Sci.*, 2021, **22**(4), 1–15.

54 J. Czechowska, E. Cichoń, A. Belcarz, A. Ślósarczyk and A. Zima, Effect of gold nanoparticles and silicon on the bioactivity and antibacterial properties of hydroxyapatite/chitosan/tricalcium phosphate-based biomicroconcretes, *Materials*, 2021, **14**(14), 3854.

55 A. Machul, D. Mikołajczyk, A. Regiel-Futyra, P. B. Heczko, M. Strus, M. Arruebo, *et al.*, Study on inhibitory activity of chitosan-based materials against biofilm producing Pseudomonas aeruginosa strains, *J. Biomater. Appl.*, 2015, **30**(3), 269–278.

56 M. H. Siddique, B. Aslam, M. Imran, A. Ashraf, H. Nadeem, S. Hayat, *et al.*, Effect of Silver Nanoparticles on Biofilm Formation and EPS Production of Multidrug-Resistant Klebsiella pneumoniae, *BioMed Res. Int.*, 2020, 2020.

57 K. Kalishwaralal, S. BarathManiKanth, S. R. K. Pandian, V. Deepak and S. Gurunathan, Silver nanoparticles impede the biofilm formation by Pseudomonas aeruginosa and Staphylococcus epidermidis, *Colloids Surf. B Biointerfaces*, 2010, **79**(2), 340–344.

58 A. Banu, M. M. Noorul Hassan, J. Rajkumar and S. Srinivasa, Spectrum of bacteria associated with diabetic foot ulcer and biofilm formation: a prospective study, *Australas. Med. J.*, 2015, **8**(9), 280–285.

59 F. Martinez-Gutierrez, L. Boegli, A. Agostinho, E. M. Sánchez, H. Bach, F. Ruiz, *et al.*, Anti-biofilm activity of silver

nanoparticles against different microorganisms, *Biofouling*, 2013, **29**(6), 651–660.

60 S. Rachid, K. Ohlsen, W. Witte, J. Jo¨, J. Hacker and W. Ziebuhr, *Effect of Subinhibitory Antibiotic Concentrations on Polysaccharide Intercellular Adhesin Expression in Biofilm-Forming Staphylococcus epidermidis*, vol. 44, 2000, available from: **https://aac.asm.org/**.

61 B. Orgaz, M. M. Lobete, C. H. Puga and C. S. Jose, Effectiveness of chitosan against mature biofilms formed by food related bacteria, *Int. J. Mol. Sci.*, 2011, **12**(1), 817–828.

62 Y. Cao, Y. F. Tan, Y. S. Wong, M. W. J. Liew and S. Venkatraman, Recent advances in chitosan-based carriers for gene delivery, *Mar. Drugs*, 2019, **17**(6), 381.

63 M. H. Siddique, B. Aslam, M. Imran, A. Ashraf, H. Nadeem, S. Hayat, *et al.*, Effect of Silver Nanoparticles on Biofilm Formation and EPS Production of Multidrug-Resistant Klebsiella pneumoniae, *BioMed Res. Int.*, 2020, 2020.